Journal of Power Sources 182 (2008) 112–118

Contents lists available at ScienceDirect

Journal of Power Sources

journal homepage: www.elsevier.com/locate/jpowsour

Short communication

Effect of capillary pressure on liquid water removal in the cathode gas diffusion layer of a polymer electrolyte fuel cell

Wanyuan Shi [a,b,*], Eru Kurihara [b], Nobuyuki Oshima [b]

[a] College of Power Engineering, Chongqing University, China
[b] Graduate School of Engineering, Hokkaido University, Kita-13, Nishi-8, Kita-ku, Sapporo 060-8628, Japan

ARTICLE INFO

Article history:
Received 29 December 2007
Received in revised form 10 March 2008
Accepted 22 March 2008
Available online 29 March 2008

Keywords:
Polymer electrolyte fuel cell
Capillary pressure
Temperature
Liquid water
Gas diffusion layer

ABSTRACT

In order to investigate the effect of capillary pressure on the transport of liquid water in the cathode gas diffusion layer (GDL) of a polymer electrolyte fuel cell, a one-dimensional steady-state mathematical model was developed, including the effect of temperature on the capillary pressure. Numerical results indicate that the liquid water saturation significantly increases with increases in the operating temperature of the fuel cell. An elevated operating temperature has an undesirable influence on the removal of liquid water inside the GDL. A reported peculiar phenomenon in which the flooding of the fuel cell under a high operating temperature and an over-saturated environment is more serious in a GDL combined with a micro-porous layer (MPL) than in a GDL without an MPL [Lim and Wang, Electrochim. Acta 49 (2004), 4149–4156] is explained based on the present analysis.

1. Introduction

In polymer electrolyte fuel cells (PEFC), excessive liquid water remaining inside the gas diffusion layer (GDL), catalyst layer (CL) or even in the gas channel tends to inhibit the performance of the fuel cell, especially at a high current density. This phenomenon, commonly called flooding [1], is confirmed to be more serious in the cathode GDL than in the GDL on the anode side [2]. Though the GDL is commonly wet-proof treated by adding polytetrafluroethylene (PTFE) to increase its hydrophobicity or combined with a very highly hydrophobic micro-porous layer (MPL), the flooding still appears or is even more serious under some performance conditions than it with a lower PTFE content or in a GDL without an MPL [3,4]. Thus, further understanding of the mechanism of liquid water transport inside the GDL is very critical.

Within the past decade, several experimental, numerical, and analytical investigations of water removal have been performed [5–9]. There are two kinds of opinions regarding the mechanism of liquid water transport inside the hydrophobic GDL. Nam and Kaviany suggested based on their theoretical analysis that the distribution of water showed a branching-type geometry [5]. They considered that water vapor condenses at the surface into micro-droplets, which intermittently agglomerate to macro-droplets of liquid water. In their model, the large main streams extend and branch into many small streams from the CL to the channel side. A similar model was also described by Pasaogullari and Wang [7]. This kind of model was termed an "upside-down tree" or "inverted tree" capillary network by Litster and Djilali [9,10], in order to distinguish it from another transport model that they proposed themselves based on their ex situ experimental observation using a fluorescence microscope [9]. In contrast to the "upside-down tree" model, they proposed a mechanism in which the accumulation of liquid water generated by the oxygen reduction reaction (ORR) builds up liquid pressure and preferentially breaks through the pores with the greatest diameter. A dominated pathway is formed after the liquid water penetrates through the GDL along the thickness direction. Meanwhile, numerous "dead ends" exist inside the GDL, where an adjacent breakthrough channel forms. In fact, a similar model was proposed by Yang et al. [11] earlier than Litster et al. [9]. Yang et al. believed that some preferential openings are connected to a network of large hydrophilic pores inside the GDL to form a pathway for liquid water transport [11].

Though these two models differ in their details, they share the concept that the capillary action resulting from the capillary pressure distribution plays a dominant role in the transport of liquid water inside the GDL. Djilali [10] also proposed that liquid water transport is dominated by means of capillary diffusion because the capillary number (the ratio of viscous forces to surface tension forces) is generally small.

* Corresponding author at: College of Power Engineering, Chongqing University, Chongqing 400030, China. Tel.: +86 23 65102471.
E-mail address: wanyuanshi@yahoo.com.cn (W. Shi).

0378-7753/$ – see front matter © 2008 Elsevier B.V. All rights reserved.
doi:10.1016/j.jpowsour.2008.03.056

Nomenclature

F	Faraday constant ($C\,mol^{-1}$)
h	heat transfer coefficient ($W(m^2\,K)^{-1}$)
I	current density ($A\,cm^{-2}$)
J	Leverett function
K	permeability (m^2)
K_{rl}	relative permeability
M_{H_2O}	molecular weight of water ($kg\,mol^{-1}$)
n_{e^-}	stoichiometry coefficient of electron in cathode reaction
Nu	Nusselt number
P_c	capillary pressure (Pa)
q	heat flux ($W\,m^{-2}$)
s	saturation of liquid water
ΔS_c	entropy change of oxygen reduction reaction ($J\,(mol\,K)^{-1}$)
T	temperature
x	x coordinate (m)

Greek symbols

β	constant in capillary pressure versus temperature equation (K^{-1})
λ	thermal conductivity ($W\,m^{-1}\,K^{-1}$)
δ	thickness (m)
ε	porosity of porous medium
η	over-potential (V)
θ	contact angle
ν	kinematic viscosity ($m^2\,s^{-1}$)
σ	surface tension ($N\,m^{-1}$)

Subscripts

c	cathode
f	fluid
g	gas phase
l	liquid phase
L	land of bipolar plate, or left hand side
MPL	micro-porous layer
nw	non-wetting phase
r	reference value
R	right hand side

Based on this common idea, some investigations of the liquid water distribution in GDL and the effect of capillary pressure were carried out numerically or analytically. Nam and Kaviany [5] assumed that water vapor (or steam) is produced by a reaction on the cathode CL surface. The phase change of the water accompanies its transport. Driven by capillary pressure, condensed liquid water flows from a location with higher liquid water saturation (volume fraction of the open pore spaces occupied by liquid water) to a point with lower saturation. They analyzed the liquid water saturation distribution and the effects of the porosity and permeability of the GDL. They also compared the capillary pressure and liquid water saturation in a GDL with an MPL (micro-porous layer) with those in a GDL without an MPL. In contrast, Pasaogullari and coworkers [2,7] considered that liquid phase water was produced on the cathode CL surface. The phase change was neglected in their one-dimensional model. They obtained the liquid water saturation distribution inside the GDL and MPL by an analytical solution and discussed the effect of the contact angle of the water. Similar work was performed by Zhan et al. [12,13]. These analyses were based on a simplified one-dimensional model; however, they can predict the liquid water saturation distribution inside the GDL along the thickness direction, which is very difficult up to now either by optical diagnostics [9,11,14,15] or by neutron radiography measurement [16–18]. By two-dimensional numerical simulation, Natarajan and Nguyen [19] calculated the liquid water saturation distribution using a capillary pressure–saturation relationship proposed by them. They found that the saturation at the catalyst layer is close to 100%. But they neglected the effect of temperature on capillary pressure. Berning and Djilali [20] found that the liquid water saturation decreases from the catalyst layer towards the gas channel, which is similar to that reported by You and Liu [21].

In a porous medium, the capillary pressure is related to the surface tension and the contact angle (or wetting coefficient) of the fluid on the solid surface. It is important to emphasize that both surface tension and contact angle are decreasing functions of temperature [22–24]. Consequently, the capillary pressure in the porous medium tends to decrease with increases in temperature [22–24]. For example, the relative decrease in capillary pressure is typically about $-1\%\,K^{-1}$ in porous media samples fashioned from soils, rocks, etc. [23]. In most of the reported analytical solutions or two-phase numerical models of liquid water transport in the PEFC, only the effect of temperature on the surface tension of the air–water system is usually considered [25,26], whereas the influence of temperature on the contact angle is usually ignored. Recently, Kumbur et al. [27] experimentally measured the capillary pressure–saturation relationship for several commercial GDL samples at different temperatures and found that the capillary pressure decreases with increases in temperature. In an empirical correlation of the capillary pressure–saturation relationship that they proposed the effect of temperature was introduced explicitly. One distinctive feature of their empirical correlation is that no contact angle parameter is required as an input except for the PTFE weight percentage of GDL. They claimed that their empirical correlation successfully predicted the capillary pressure over the entire range of saturation. However, the figures in their paper show that their correlation is not highly consistent with their experimental data for most of the GDL samples used for their experiments when the saturation is less than 0.1. In particular, when the saturation is very small, such as less than 0.01, their empirical correlation predicts negative capillary pressure values for a hydrophobic GDL with 5 wt.% PTFE, which is physically incorrect. In fact, for a GDL working in an actual PEFC, the water saturation is mostly less than 0.1, and serious flooding occurs if the saturation is higher than 0.1 [7]. In contrast, the standard Leverett function can avoid such error even for very low levels of saturation, although it is originally derived from soil science.

In this work, we propose a one-dimensional steady-state mathematical model based on a capillary pressure–saturation relationship, including the influence of temperature, using the standard Leverett function. The influence of temperature on the liquid water saturation is investigated numerically inside the cathode GDL. The phenomenon related to liquid water transport reported in the literature is discussed based on the present analyses.

2. Physical and mathematical models

As mentioned in the previous section, flooding usually occurs more seriously in the GDL at the cathode side than that at the anode side. Thus, the present study only considers the water transport in the GDL at the cathode side. A schematic physical model is shown in Fig. 1. In the cathode catalyst layer, the water and heat are generated due to the oxygen reduction reaction:

$$4H^+ + O_2\,(g) + 4e^- \rightarrow 2H_2O\,(l). \quad (1)$$

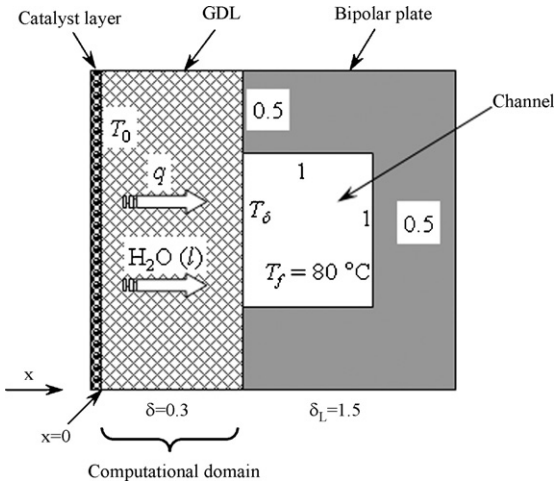

Fig. 1. Physical model.

Here, the generated water is assumed to be in the liquid phase. The phase change of the water is neglected for the purpose of simplification; thus, the water substance is transported in the GDL in the liquid single phase. Heat convection due to gas and liquid water flow inside the GDL is also ignored. The CL is assumed to be an infinitely thin layer, and is also assumed to act as an adiabatic boundary because of its small thermal conductivity in comparison with that of the GDL [28]. Therefore, all of the heat generated at the catalyst layer is transferred to the gas flowing in the gas channel and bipolar plate by heat conduction. Under a steady state, a one-dimensional energy conservation equation and boundary conditions are expressed as follows:

$$q = -\lambda \frac{dT}{dx}. \tag{2a}$$

$$\text{At} \quad x = 0: \quad q = \left(\frac{-\Delta S_c T_0}{n_{e^-} F} + \eta_c \right) I. \tag{2b}$$

$$\text{At} \quad x = \delta: \quad q = \frac{h(T_\delta - T_f)}{2} + \frac{\lambda_L (T_\delta - T_f)}{2\delta_L}. \tag{2c}$$

In Eq. (2b), ΔS_c is the entropy change in the reaction of Eq. (1), which represents the reversible heat generation. $\Delta S_c = -326.36\,\text{J}\,(\text{mol K})^{-1}$ indicates that the reaction is exothermic [29]. η_c is the over-potential of the cathode CL, which represents the heat generation due to irreversible operation (i.e., effective losses) [28,30]. Where T_0 is the temperature at the interface between the CL and GDL (i.e., at $x = 0$), which equals the temperature of the CL. n_{e^-} is the stoichiometry coefficient of the electron and $n_{e^-} = 4$ from Eq. (1). I is the average current density. On the GDL surface facing the gas (air) channel (i.e., at $x = \delta$, the heat convection is represented by heat-transfer coefficient h, which is given from the Nusselt number (Nu)). The value of h is calculated to be $106.1\,\text{W}\,(\text{m}^2\,\text{K})^{-1}$ for the air flow because Nu is constant and equals 3.61 for laminar flow in the square duct under constant heat flux [31]. T_δ and T_f are the temperatures at the GDL–channel interface ($x = \delta$) and the bulk temperature of the gas in the gas channel, respectively. The temperature at the right side wall of the bipolar plate is also assumed to be T_f. The thermal conductivities of the GDL, bipolar plate and air in the channel are listed in Table 1. For a porous GDL, an effective thermal conductivity of the pores and solid regions in combination is applied [37]. Here, a low thermal conductivity of the GDL is utilized, considering the fact that the thermal conductivity of the GDL decreases with increases in temperature and PTFE content [38].

Table 1
Parameters of calculation

Geometry size (mm)	
Thickness of GDL with/without MPL (δ)	0.27/0.3
Channel width/height	1/1
Bipolar plate thickness δ_L/height	1.5/2
Thickness of MPL	0.03 [2]
Thermal conductivity ($\text{W m}^{-1}\,\text{K}^{-1}$)	
GDL (λ) (effective)	0.75 [32]
Air (λ_{air})	0.0294 [33]
Bipolar plate (λ_L)	20 [26]
Faraday constant (F)	$96487\,\text{C mol}^{-1}$
Molecular weight of water (M_{H_2O})	$18.0 \times 10^{-3}\,\text{kg mol}^{-1}$
Surface tension of liquid water at 25 °C (σ)	$0.0725\,\text{N m}^{-1}$ [34]
Contact angle of water at 25 °C unless specifically mentioned (θ)	112°
Viscosity of liquid water (ν)	$3.5 \times 10^{-7}\,\text{m}^2\,\text{s}^{-1}$ [2]
Porosity of GDL (ε)	0.78 [34]
Porosity of MPL (ε_{MPL})	0.5 [2]
Single phase permeability of GDL (K)	$8.99 \times 10^{-12}\,\text{m}^2$ [35]
Single phase permeability of MPL (K_{MPL})	$2.47 \times 10^{-16}\,\text{m}^2$ [2]
Gas temperature in channel (T_f)	80 °C
Cathode over-potential (η_c)	0.4 V [36]
Current density (I)	$1.0\,\text{A cm}^{-2}$

The capillary pressure is defined as the difference between liquid and gas-phase pressures:

$$P_c = P_l - P_g. \tag{3}$$

If the gas phase pressure inside the GDL is assumed to be constant at P_g, which is equal to the environmental pressure, P_c may be considered a relative pressure head of liquid water. In hydrophobic porous media, $P_c > 0$, i.e., the liquid-phase pressure, is higher than the gas-phase pressure, whereas in hydrophilic media, the liquid-phase pressure is lower than the gas-phase pressure ($P_c < 0$). Furthermore, in hydrophobic porous media, the magnitude of the capillary pressure increases with the increase of the liquid water saturation. Therefore, a liquid pressure drop is formed from high to low liquid saturation regions, which is an important driven force for liquid water transport. In many reports [2,7,25,26], Eq. (4) is adopted for the capillary pressure as a function of non-wetting phase saturation (s_{nw}).

$$P_c(T_r) = -\frac{\sigma \cos\theta}{(K/\varepsilon)^{1/2}} J(s_{nw}). \tag{4}$$

The minus symbol is imposed to match with our definition of capillary pressure, i.e., Eq. (3). In Eq. (4), $J(s_{nw})$ is the Leverett function, which was originally regressed by Udell [39] based on the experimentally obtained capillary pressure data sets in unconsolidated sands reported by Leverett [40]. The Leverett function was extended to hydrophobic porous media by Nam and Kaviany [5] and Pasaogullari and Wang [7] for the fuel cell transport model. The s_{nw} is defined as the volume fraction of the void occupied by the non-wetting phase. In hydrophobic media, the non-wetting phase is liquid water, i.e., $s_{nw} = s$, whereas in hydrophilic media, the non-wetting phase is air, and $s_{nw} = 1 - s$. Here, s indicates the saturation of liquid water, which is defined as

$$s = \frac{V_{liquid}}{V_{pore}}. \tag{5}$$

Then, the $J(s)$ function is expressed as [7]:

$$J(s) = \begin{cases} 1.417(1-s) - 2.12(1-s)^2 \\ \quad +1.263(1-s)^3, & \text{for} \quad 0 < \theta < 90^\circ \\ 1.417s - 2.12s^2 + 1.263s^3, & \text{for} \quad 90^\circ < \theta < 180^\circ \end{cases} \tag{6}$$

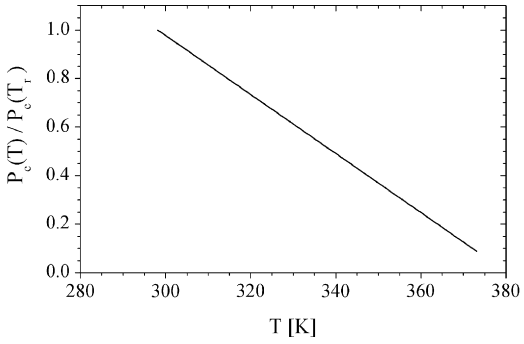

Fig. 2. Capillary pressure as a function of temperature [22].

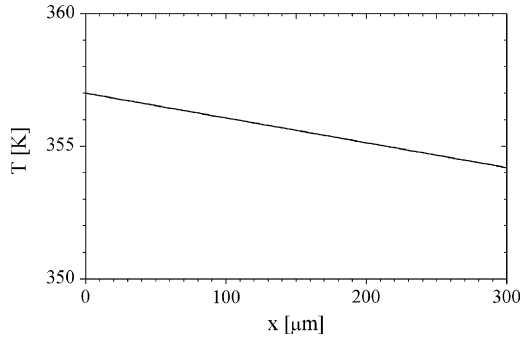

Fig. 3. Temperature as a function of distance along the GDL thickness at $T_f = 353$ K.

where θ is the contact angle of liquid on a flat surface. For hydrophilic surfaces, θ ranges from $0 < \theta < 90^\circ$, while $90^\circ < \theta < 180^\circ$ for hydrophobic surfaces.

In the electrolyte membrane, the water flux driven by electro-osmotic drag is assumed to be balanced by backing diffusion at steady state, i.e., there is no water leakage from the electrolyte membrane. All of the water generated in CL must be transported through GDL by capillary pressure toward the gas channel. For simplification, assuming that the phase change of water inside the GDL and the effect of gravitation are negligible, Darcy's law can be expressed as [7]:

$$\frac{I}{2F} M_{H_2O} = -\frac{k_{rl} K}{\nu} \nabla P_c(T), \tag{7}$$

where F is the Faraday constant, M_{H_2O} is the molecular weight of water, ν is the viscosity of liquid water, K is the absolute permeability of GDL and k_{rl} is the relative permeability for liquid water. The relative permeability can be determined by means of experiment [34] or pore network modeling [41,42]. In this work, the GDL is assumed to be isotropic and homogeneous porous medium, and the relative permeability of individual phase is assumed to be proportional to the cube of individual phase saturation [7]. For liquid water, it is known as

$$k_{rl} = s^3. \tag{8}$$

A boundary condition for Eq. (7) is given at the GDL surface facing the gas channel (at $x = \delta$). In general, a constant value is assigned for the liquid water saturation at $x = \delta$ [5,7,12,13]. Here, $s = 0$ is assumed at $x = \delta$:

$$\text{at } x = \delta: \quad s = 0. \tag{9}$$

The effect of temperature on capillary pressure is expressed by a formula proposed by Grant [22,23], as follows:

$$P_c(T) = P_c(T_r) \frac{\beta + T}{\beta + T_r}, \tag{10}$$

where $P_c(T_r)$ is capillary pressure at a reference temperature (T_r). Here, $T_r = 298$ K is used for the following analysis. β is a constant related to porous medium [22]. Due to lack of experimental data for GDL, the constant $\beta = -380.4$ K was adopted, which was determined from experimental data of air–water drainage in a silt loam [22]. Fig. 2 shows the P_c versus temperature profile. It is worthwhile to emphasize that the influence of temperature on both surface tension and contact angle have been considered in Eq. (10) [22]. Therefore, it is not necessary to consider the effect of temperature on the surface tension or the contact angle individually, which is an important advantage because the effect of temperature on the contact angle of GDL is not well known. Recently, similar method has been adopted by Kumbur et al. [27]. Thus, Eq. (10) is employed priorly in the following calculations, i.e., the constant surface tension and the constant contact angle values at the reference temperature (298 K) are required in the Eq. (4) unless specified otherwise. Eq. (10) is introduced into Eq. (7), and then liquid water conservation is expressed as

$$\frac{I}{2F} M_{H_2O} = -\frac{k_{rl} K}{\nu} \nabla \left[\frac{\beta + T}{\beta + T_r} P_c(T_r) \right]. \tag{11}$$

In the analysis of GDL combined with MPL, the liquid water saturation at the interface between MPL and GDL is determined from phenomena of capillary equilibrium expressed by the following equation:

$$\frac{\cos(\theta)}{(K/\varepsilon)^{1/2}} J(s) = \frac{\cos(\theta_{MPL})}{(K_{MPL}/\varepsilon_{MPL})^{1/2}} J(s_{MPL}). \tag{12}$$

3. Results and discussion

3.1. Temperature field in GDL

The analytical solution of (2) is

$$T = -\frac{q}{\lambda} x + T_0. \tag{13a}$$

$$\text{And } T_0 = \frac{T_f + [\delta/\lambda + 1/(0.5h + 0.5\lambda_L/\delta_L)]\eta_c I}{1 + [\delta/\lambda + 1/(0.5h + 0.5\lambda_L/\delta_L)]\Delta S_c I/(n_{e^-} F)}. \tag{13b}$$

Under the operation condition given by $T_f = 353$ K, $\eta_c = 0.4$ V, $I = 1.0$ A cm^{-2} and the other parameters listed in Table 1, we obtain $T_0 = 357.0$ K and $T_\delta = 354.2$ K, and the temperature field in GDL is shown in Fig. 3. The temperature difference between the two sides of the GDL is 2.8 K, which falls in the same range of temperature drop as that described in the literature [38].

3.2. Saturation and capillary pressure inside GDL

Substituting Eqs. (4) and (6) into Eq. (11), the liquid water saturation in a one-dimensional model is expressed as follows:

$$s^3(-3.789s^2 + 3.338s - 0.966)\frac{ds}{dx} = f, \quad \text{for } \theta < 90^\circ \tag{14a}$$

$$s^3(3.789s^2 - 4.24s + 1.417)\frac{ds}{dx} = f, \quad \text{for } \theta > 90^\circ, \tag{14b}$$

where

$$f = \frac{A(\beta + T_r)}{\beta + T} + \frac{J(s)s^3}{(\beta + T)}\frac{q}{\lambda}, \tag{14c}$$

and

$$A = \frac{I M_{H_2O}}{2F} \frac{\nu}{(K\varepsilon)^{1/2}\sigma\cos(\theta)}. \tag{14d}$$

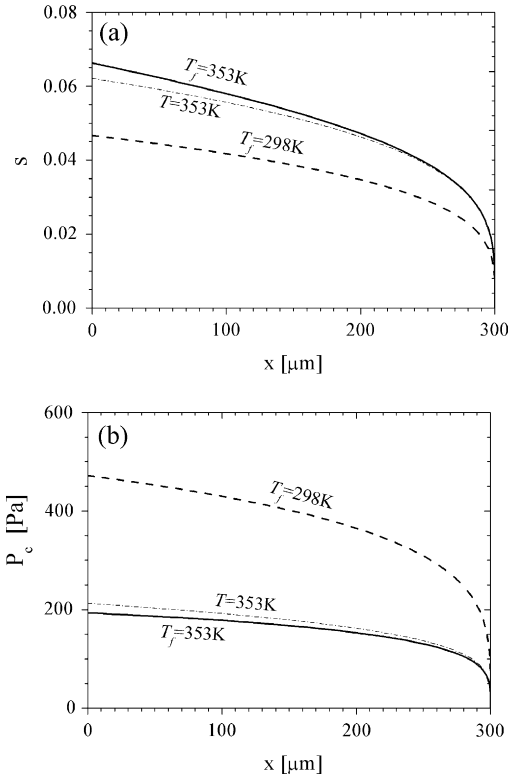

Fig. 4. (a) Liquid water saturation and (b) capillary pressure profiles across the GDL thickness at 298 K and 353 K. Solid lines: the temperature gradient is considered in Eq. (14c). Dash–dot lines: the temperature gradient is neglected, i.e., $q = 0$ in Eq. (14c).

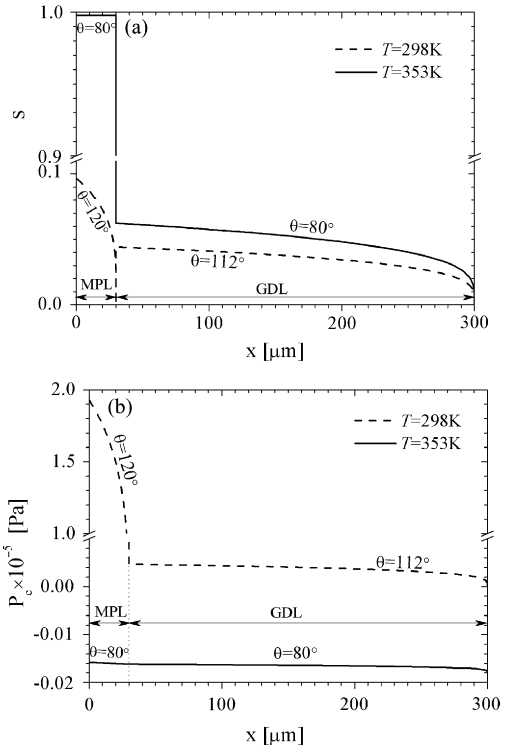

Fig. 5. (a) Liquid water saturation and (b) capillary pressure profiles across the thickness of the GDL with an MPL at 298 K and 353 K.

The local saturation, $s(x)$, can be obtained by numerically solving (14). The capillary pressure distribution can then be calculated from Eq. (10). For example, when $\eta_c = 0.4$ V, $I = 1.0$ A cm^{-2} and the contact angle $\theta = 112^\circ$, the liquid water saturations under different temperature conditions are as shown in Fig. 4a. Since the capillary pressure decreases with an increase in temperature, s at $T_f = 353$ K (air temperature in the gas channel) is significantly higher than that at the room temperature of air ($T_f = 298$ K). In particular, $s(0)$, i.e., the water saturation at the interface between CL and GDL (at $x = 0$), for $T_f = 353$ K is about 41.9% higher than that for $T_f = 298$ K. The capillary pressure profile changes as shown in Fig. 4b. At the interface between CL and GDL (at $x = 0$), $P_c(0)$ for $T_f = 353$ K is as low as 41.0% of that for $T_f = 298$ K. This result clearly indicates that elevation of the operating temperature significantly reduces the liquid water removal ability of porous GDL, increases the water saturation in the entire volume of GDL, suppresses the gas permeability and eventually causes flooding. All of these influences decrease fuel cell performance. This effect of operating temperature has not been well recognized in the reported literature [2,5,7,12,13], although Weber and Newman found that the performance of fuel cell may become worse at high operating temperature [28].

By solving (14) without the temperature gradient, i.e., neglecting the second term in Eq. (14c), we can evaluate the effect of the non-uniformity of temperature on the distributions of water saturation and capillary pressure as shown by the dash–dot lines in Fig. 4. The results indicate that the temperature gradient in the GDL has a small influence on the saturation and capillary pressure distributions because of the small temperature difference despite the large temperature gradient in the GDL (9.3×10^3 K m^{-1}). We speculate that the similar conclusion is also valid for anode GDL, MPL, membrane as well as catalyst layer because of their thin thickness too. Therefore, we neglect the effect of temperature gradient in the following calculation.

It is well known that a micro-porous layer with high hydrophobicity, low permeability and small pore diameter can usually significantly improve the limitation of mass loss and effectively avoid flooding [43,44]. As an example, an MPL with a thickness $\delta_{MPL} = 30$ μm is introduced here, and the operating temperature of the fuel cell is assumed to be uniform at 298 K. The contact angle $\theta = 112^\circ$ for the GDL and $\theta = 120^\circ$ for the MPL, and the surface tension $\sigma = 0.0725$ N m^{-1} at 298 K. The other parameters are tabulated in Table 1. At the interface between the MPL and GDL, the saturation must satisfy Eq. (12). As shown in Fig. 5a, the liquid water saturation inside the main part of the MPL is higher than that in the GDL. A very large capillary pressure gradient is generated near the interface between the MPL and GDL, as shown in Fig. 5b, which is effective for draining liquid water from the CL through the MPL and toward the gas channel. The high capillary pressure is one of the significant advantages in comparing with other factors, such as low ohmic losses [44].

As a typical example referred to in some reports [2,43,44], Qi and Kaufman [43] found that MPL significantly improves the performance of fuel cells at a low cell operating temperature (308 K), increasing the limiting current up to 0.6 A cm^{-2} at 0.4 V when air is utilized as a cathode reactant. In contrast, Lim and Wang [3] found that, in a peculiar phenomenon, the MPL reduces the performance of the fuel cell, i.e., the limiting current density of the fuel cell is lower (about 0.33 A cm^{-2} at 0.4 V) than that without the MPL, although the fuel cell was operated at similar reactant stoichiometry and air-fed as the cathode reactant, using similar wet-proof carbon paper as the GDL except at the higher operating temperature (353 K) and in an over-saturated environment (hydrogen and air humidified at 368 K and 363 K, respectively). Such a low limita-

tion current indicates that flooding occurred. They explained briefly that the MPL imposed an additional diffusion resistance to oxygen transport into the catalyst layer, and the mass transport rate limited the current [3]. However, they did not explain the reason for the additional diffusion resistance. The higher current density under a low operating temperature indicates that the reaction proceeded faster and that more water was generated than in the latter case operated at a higher temperature. However, flooding occurred at the latter case regardless of its lower water generation rate. This may be attributed to the decrease of the driven force of liquid water transportation in the MPL and GDL, i.e., the capillary pressure gradient at the higher temperature. Under a high operating temperature, even under a low reaction rate, the generated water could not be drained, but rather accumulated inside the GDL and MPL, which increased the diffusion resistance of oxygen transport and further decreased the reaction rate.

In fact, in Lim and Wang's work [3], it was found that the contact angle of GDL rapidly decreased from 98° to 108° (hydrophobic) to 80° (hydrophilic) as the temperature increased from 298 K to 353 K. At temperatures above 313 K, even a 40-wt.% FEP-treated hydrophobic GDL became hydrophilic [3]. Although their measurement of the contact angle was focused only on a normal GDL, here, we assume that a similar phenomenon occurs in the MPL. Recently, Kumbur et al. [27] experimentally found that the hydrophilic pore volume of hydrophobic treated GDL increased with increasing temperature, especially for macropores (radius range from 1 μm to 100 μm). They suggested that the temperature has a small effect on the wettability characteristics of MPL due to the minute pores restricting the imbibition of water, therefore impeding observation of the apparent effects of temperature on the pore characteristics of the MPL. However, the water vapor can enter the minute pores of the MPL. After the steam condensed, the liquid water remained in the minute pores of the MPL. If so, the temperature should also have apparent effects on the pore characteristics of the MPL. Here, we assumed that both the surface tension and the contact angle of the GDL as well as the MPL decrease with increasing temperature. At 353 K, their surface tension was 0.0625 N m^{-1} [2]. The contact angle was assumed to be 80° for the GDL and MPL surfaces. Because the values of the surface tension and the contact angle had already incorporated the effect of temperature individually, it was not necessary to apply Eq. (10) also. As a special case, the liquid water saturation was solved by Eq. (7). As shown in Fig. 5, the saturation was significantly higher than that in the GDL + MPL operated at room temperature. In particular, the saturation in the MPL was close to 1, i.e., the MPL pores were almost entirely occupied by liquid water. In order to maintain the capillary pressure equilibrium at the interface of the GDL and MPL, a high saturation is necessary in the MPL because of its minute effective pore diameter, i.e., $(K/\varepsilon)^{1/2}$. Obviously, serious flooding would occur in such a case. This is a possible reason why Lim and Wang found that MPL has an undesirable influence on the performance of fuel cells at high cell temperatures and in an over-saturated environment. Because the wettability of the GDL and MPL become hydrophilic, the capillary pressure is negative at 353 K.

Finally, we would like to emphasize that the phase change of water was neglected in this work for the purpose of simplification. We noted that Weber and Newman [28] have found that the evaporation and condensation of water caused a significant movement of water, mainly through heat-pipe effect. The phase change of water was also considered in the models proposed by Nguyen's group [19,45], Nam and Kaviany [5], Mazumder and Cole [46]. Therefore, a coupled model including the temperature influence on capillary pressure as well as phase change is necessary for the future research on the water removal in the fuel cells.

4. Conclusions

In a one-dimensional steady-state model including the effect of temperature on the capillary pressure, the liquid water saturation and capillary pressure distributions were investigated in the cathode GDL of a PEFC. The numerical results indicate that liquid water saturation significantly increases with increases in the operating temperature of the fuel cell. An elevated operating temperature has an undesirable influence on the removal of liquid water inside the GDL. A reported peculiar phenomenon, that the flooding of a fuel cell operated under high temperature and in an over-saturated environment is more serious in a GDL combined with an MPL than in a GDL without an MPL is explained based on the present analysis.

Acknowledgements

A financial support for this research from NEDO (New Energy and Industrial Technology Development Organization) of Japan is gratefully acknowledged. Authors thanks Dr. N. Imaishi, Professor Emeritus of Kyushu University, for his helpful comments. We would also like to thank Mr. L.K. Saha for his useful discussion.

References

[1] Z.H. Wang, C.Y. Wang, K.S. Chen, J. Power Sources 94 (2001) 40–50.
[2] U. Pasaogullari, C.-Y. Wang, K.S. Chen, J. Electrochem. Soc. 152 (2005) A1574–A1582.
[3] C. Lim, C.Y. Wang, Electrochim. Acta 49 (2004) 4149–4156.
[4] G. Lin, T.V. Nguyen, J. Electrochem. Soc. 152 (2005) A1942–A1948.
[5] J.H. Nam, M. Kaviany, Int. J. Heat Mass Transfer 46 (2003) 4595–4611.
[6] C.Y. Wang, Chem. Rev. 104 (2004) 4727–4766.
[7] U. Pasaogullari, C.Y. Wang, J. Electrochem. Soc. 151 (2004) A399–A406.
[8] P.K. Sinha, P.P. Mukherjee, C.-Y. Wang, J. Mater. Chem. 17 (2007) 3089–3103.
[9] S. Litster, D. Sinton, N. Djilali, J. Power Sources 154 (2006) 95–105.
[10] N. Djilali, Energy 32 (2007) 269–280.
[11] X.G. Yang, F.Y. Zhang, A.L. Lubawy, C.Y. Wang, Electrochem. Solid-State Lett. 7 (2004) A408–A411.
[12] Z. Zhan, J. Xiao, D. Li, M. Pan, R. Yuan, J. Power Sources 160 (2006) 1041–1048.
[13] Z. Zhan, J. Xiao, Y. Zhang, M. Pan, R. Yuan, Int. J. Hydrogen Energy 32 (2007) 4443–4451.
[14] F.Y. Zhang, X.G. Yang, C.Y. Wang, J. Electrochem. Soc. 153 (2006) A225–A232.
[15] P.K. Sinha, P. Halleck, C.-Y. Wang, Electrochem. Solid-State Lett. 9 (2006) A344–A348.
[16] R. Satija, D.L. Jacobson, M. Arif, S.A. Werner, J. Power Sources 129 (2004) 238–245.
[17] D. Kramer, J. Zhang, R. Shimoi, E. Lehmann, A. Wokaun, K. Shinohara, G.G. Scherer, Electrochim. Acta 50 (2005) 2603–2614.
[18] A. Turhan, K. Heller, J.S. Brenizer, M.M. Mench, J. Power Sources 160 (2006) 1195–1203.
[19] D. Natarajan, T.V. Nguyen, J. Electrochem. Soc. 148 (2001) A1324–A1335.
[20] T. Berning, N. Djilali, J. Electrochem. Soc. 150 (2003) A1589–A1598.
[21] L. You, H. Liu, Int. J. Heat Mass Transfer 45 (2002) 2277–2287.
[22] S.A. Grant, Water Resour. Res. 32 (1996) 261–270.
[23] S.A. Grant, Water Resour. Res. 39 (2003) 1–10 (SBH).
[24] H.Y. She, B.E. Sleep, Water Resour. Res. 34 (1998) 2587–2597.
[25] H. Meng, C.-Y. Wang, J. Electrochem. Soc. 152 (2005) A1733–A1741.
[26] Y. Wang, C.-Y. Wang, J. Electrochem. Soc. 153 (2006) A1193–A1200.
[27] E.C. Kumbur, K.V. Sharp, M.M. Mench, J. Electrochem. Soc. 154 (2007) B1315–B1324.
[28] A.Z. Weber, J. Newman, J. Electrochem. Soc. 153 (2006) A2205–A2214.
[29] M.J. Lampinen, M. Fomino, J. Electrochem. Soc. 140 (1993) 3537–3546.
[30] T. Berning, D.M. Lu, N. Djilali, J. Power Sources 106 (2002) 284–294.
[31] R.K. Shah, A.L. London, Advances in Heat Transfer (Suppl. 1), Academic Press, New York, 1978, pp. 78–384.
[32] H. Ju, C.-Y. Wang, S. Cleghorn, U. Beuscher, J. Electrochem. Soc. 153 (2006) A249–A254.
[33] H. Ju, C.-Y. Wang, S. Cleghorn, U. Beuscher, J. Electrochem. Soc. 152 (2005) A1645–A1653.
[34] J.T. Gostick, M.W. Fowler, M.A. Ioannidis, M.D. Pritzker, Y.M. Volfkovich, A. Sakars, J. Power Sources 156 (2006) 375–387.
[35] J.T. Gostick, M.W. Fowler, M.D. Pritzker, M.A. Ioannidis, L.M. Behra, J. Power Sources 162 (2006) 228–238.
[36] H. Meng, C.-Y. Wang, J. Electrochem. Soc. 151 (2004) A358–A367.
[37] S. Mazumder, J.V. Cole, J. Electrochem. Soc. 150 (2003) A1503–A1509.
[38] M. Khandelwal, M.M. Mench, J. Power Sources 161 (2006) 1106–1115.
[39] K.S. Udell, Int. J. Heat Mass Transfer 28 (1985) 485–495.

[40] M.C. Leverett, Trans. AIME 142 (1941) 152–169.
[41] J.T. Gostick, M.A. Ioannidis, M.W. Fowler, M.D. Pritzker, J. Power Sources 173 (2007) 277–290.
[42] B. Markicevic, A. Bazylak, N. Djilali, J. Power Sources 171 (2007) 706–717.
[43] Z. Qi, A. Kaufman, J. Power Sources 109 (2002) 38–46.
[44] A.Z. Weber, J. Newman, J. Electrochem. Soc. 152 (2005) A677–A688.
[45] W. He, J.S. Yi, T.V. Nguyen, AIChE J. 46 (2000) 2053–2064.
[46] S. Mazumder, J.V. Cole, J. Electrochem. Soc. 150 (2003) A1510–A1517.